

# Improved particle concentration by cascade AC electroosmotic flow

Masahiro Motosuke · Keichi Yamasaki ·  
Akihiko Ishida · Hikaru Toki · Shinji Honami

Received: 12 April 2012 / Accepted: 14 September 2012 / Published online: 4 December 2012  
© Springer-Verlag Berlin Heidelberg 2012

**Abstract** The importance of electrokinetics in microfluidic technology has been growing owing to its versatility and simplicity in fabrication, implementation, and handling. Alternating-current electroosmosis (ACEO), which is the motion of fluid due to the ion movement by an interaction between AC electric field and an electrical double layer on the electrode surface, has a potential for a particle concentration method to detect rare samples flowing in a microchannel. This study investigates an improved ACEO-based particle concentration by cascade electrokinetic approach. Flow field induced by ACEO and accumulation behavior of particles were parametrically measured to discuss the concentrating mechanism. The accumulation of particles by ACEO can be explained by a balance between the attenuating electroosmotic flow to transport particles and the inherent diffusive motion of the particles, which is hindered due to the near-wall location. Although a parallel double-gap electrode geometry enables particles to be collected at the center of electrode very sharply, it has scattering zones with accumulated particles at sidewalls of the channel. This drawback can be overcome by applying sheath flow or introducing cascade electrode pattern upstream of the focusing zone. As a result, total concentration efficiency was 98.4 % for all the particles flowing in the cascade device. The resultant concentrated particles exist on the electrode surface within 5  $\mu\text{m}$ , and three-dimensional concentration of particle with the concentration factor as large as 700 is possible using a monolithic channel, co-planar electrode, and sheathless solution feeding. This cascade electrokinetic

method provides a new and effective preconcentrator for ultra-sensitive detection of rare samples.

**Keywords** Alternating-current electroosmosis · AC electrokinetics · Particle concentration · Preconcentration · Cascade ACEO concentrator · Rare sample detection

## 1 Introduction

The microfluidic technology has attracted considerable attention and broadened its application fields in biology, chemistry, medical, and engineering due to the advantages in small size, low consumption, easy handling, and effective reaction (Whitesides 2006; Neethirajan et al. 2011; Yeo et al. 2011). Sensitive detection or analysis in a microfluidic device has been one of the key issues because of the inherently severe condition of the detection in a miniaturized device mainly attributed to the low sample load volume or the short optical path length of the fluidic channel (Hu et al. 2010); the number of sample per a chip is often limited. Recently, a need to detect rare samples such as circulating tumor cells in blood (Nagrath et al. 2007; Sequist et al. 2009) has emerged as a challenging task. The improvement of the detection sensitivity includes developing highly sensitive detection technique or utilizing concentration methods prior to analysis. Off-line methods to concentrate samples such as precipitation and filtration using membrane are cumbersome and at risk of contamination. An appropriate on-chip concentration technique, in which the local concentration of a target sample is controlled, can reduce the noise of obtained signal and improve the detection sensitivity (Warrick et al. 2010). Focusing particles into a tight stream in the bulk flow in a microchannel is an essential step for counting, detecting, and

---

M. Motosuke (✉) · K. Yamasaki · A. Ishida · H. Toki · S. Honami  
Department of Mechanical Engineering, Tokyo University of Science, 1-14-6 Kudankita, Chiyoda-ku, Tokyo 102-0073, Japan  
e-mail: mot@rs.tus.ac.jp

sorting them resulting in signal with high signal-to-noise ratio in such as microfluidic cytometry (Chung and Kim 2007; Ateya et al. 2008; Godin et al. 2008; Sun and Morgan 2010). The on-chip preconcentration methods can be basically classified into two categories based on their concentration mechanism: static and dynamic techniques (Sueyoshi et al. 2008; Lin et al. 2011). Static techniques consist of solvent extraction, surface binding that traps analytes and porous membrane or nanostructure that stacks targets through filtering. Dynamic ones utilize additional forces such as magnetic force (Watarai et al. 2004; Pamme 2006) or electrokinetics. Field-amplified sample stacking (FASS) is performed based on velocity differences of targets in different conductive buffers (Jacobson and Ramsey 1995; Shiddiky and Shim 2007). Isotachopheresis (ITP) uses discontinuous electric field to create sharp zone of sample (Chen et al. 2006; Cui et al. 2007). Although both FASS and ITP are extensively used for molecules and ions rather than particles, they can be applied to concentrate particles. Dielectrophoresis (DEP) is a phenomenon explained as the motion of neutral materials caused by polarization effects in a nonuniform electric field (Jones 1995). DEP is mainly used by applying AC electric field because Clausius–Mossotti factor is sensitive to the frequency of electric field that can be applied to separate, sort, focus and concentrate particles (Fiedler et al. 1998; Zhang et al. 2010). AC electrokinetic approach introduces advantages over DC-based one, like electrophoresis used in FASS and ITP, such as low temperature rise due to Joule heating and less electrolysis of solution. AC electroosmosis (ACEO), which is a field-induced fluid flow generated by an interaction between the electric double layer and the tangential component of the electric field (Castellanos et al. 2003), is one of the promising techniques of particle manipulation which does not depend on electrical properties of the particle because the transportation of particle by ACEO utilizes the fluidic force. The driving force of ACEO flow is the ion movement in the electrical double layer (EDL) on an electrode subjected to AC electric field; EDL interacts with the small horizontal component of the electric field to generate a fluid motion across the surface of electrode. A schematic model of ACEO around a co-planar electrode with a gap is shown in Fig. 1. The time-averaged ACEO velocity,  $V_{ACEO}$ , on two parallel co-planar electrodes under an assumption of a linear relation between the induced surface charge and the potential is described as (Ramos et al. 1998):

$$V_{ACEO} = \Lambda \frac{\varepsilon V^2}{8\eta} \frac{\Omega^2}{\xi(1 + \Omega^2)^2} \quad (1)$$

$$\Omega = \frac{\pi \varepsilon \omega \xi}{2\lambda_D \sigma} \quad (2)$$

where  $\Lambda$  is the ratio between the total capacitance and that of the diffuse double layer,  $\varepsilon$  is fluid permittivity,  $V$  is

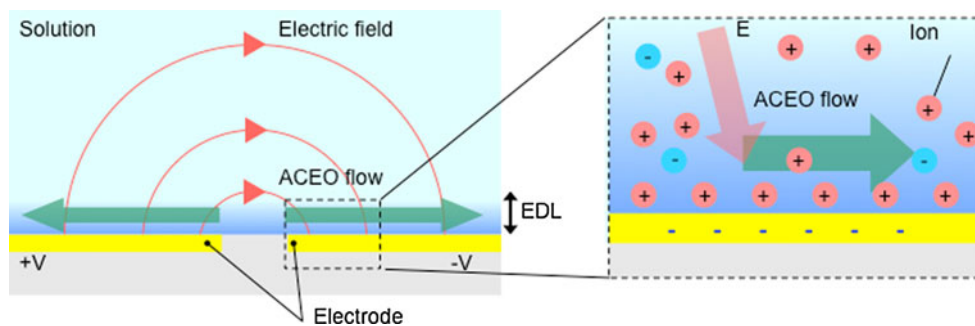
applied voltage,  $\eta$  is fluid viscosity,  $\xi$  is cross-sectional position from the center of the gap between the electrodes,  $\Omega$  is nondimensional frequency,  $\omega$  is angular frequency,  $\lambda_D$  is the Debye length and  $\sigma$  is electrical conductivity of fluid. However, this description is valid only at low voltage condition, i.e.,  $V \ll 25$  mV in a typical condition (Bazant et al. 2004) that is much smaller than practical range of several V, and the theory which can quantitatively describe the ACEO phenomenon has not been established despite tremendous efforts to describe nonlinear charge dynamics (Olesen et al. 2006; Gregersen et al. 2007; Olesen et al. 2010). Therefore, the experimental investigation of ACEO is still strongly needed to obtain its performance in application. The unique flow structure induced by ACEO enables particles to concentrate into a certain location in a microchannel with electrode array. Previous studies (Bhatt et al. 2005; Lian et al. 2006; Melvin et al. 2011) have discussed the effectiveness of particle concentration by ACEO around electrodes located at limited positions in the fluidic channel. They confirmed that ACEO could collect particles toward a specific zone on electrode depending on the geometry of the electrode array. However, effective spatial range of concentration and net efficiency of the concentration performance have not been fully evaluated. Additionally, due to the nature of ACEO, a scattering area in which particles are spread is inevitable at outer side of concentrating site. Limited knowledge of ACEO-based concentration without information about the scattering area would allow a limited application of the particle concentration technique only at localized area of the channel. To enlarge the application field of particle concentration by ACEO flow to rare sample detection (Prat et al. 2011), verification of long-ranged concentration in which all the particles flowing in the channel can be focused into single localized area is highly needed. In this study, the particle collection by ACEO for long-ranged concentration in a microfluidic channel is discussed with quantitative analysis of concentration factor. The insight can be used in the optimization of the concentrator design.

## 2 Materials and methods

### 2.1 Fluidic device

A schematic of a microfluidic device is shown in Fig. 2. It has a polydimethylsiloxane (PDMS; Sylgard 184, Dow Corning Toray, Japan) microchannel fabricated by the softlithography whose scale is 500  $\mu\text{m}$  wide and 50  $\mu\text{m}$  high. The PDMS channel was bonded to a glass substrate with transparent indium tin oxide (ITO) electrode (Geomatec, Japan) using oxygen plasma (YHS-360, SAKIGAKE-Semiconductor, Japan). The use of ITO as the

**Fig. 1** Schematic model of alternating-current electroosmosis (ACEO) generated by ion movement in diffusive layer subjected to AC electric field



electrode allows easy optical access through the substrate so that clear particle image can be observed. The electrode was placed on the glass by the sputtering, and patterning was carried out by conventional wet etching. The thickness of ITO film was approximately 90 nm. In this study, three electrode patterns, single-gap (SG), double-gap (DG), and asymmetric-branch (AS), were used as depicted in Fig. 2b. The gaps of SG and DG are 25  $\mu\text{m}$  and set parallel to the main flow direction. The center electrode in DG has width of 300  $\mu\text{m}$  and side electrode is 75  $\mu\text{m}$  wide each. AS electrode has branches of asymmetric inter-digitated electrode arrays that generate inward ACEO flow from sidewall to center area due to their asymmetric electric field strength (Ajdari 2000). The branches of AS consist of asymmetric electrode array with wide (100  $\mu\text{m}$ ) and narrow (10  $\mu\text{m}$ ) lines. The spacing between electrodes are 25  $\mu\text{m}$ . A trunk of AS is 100  $\mu\text{m}$  wide. Additionally, a cascade pattern which used both AS and DG in the same chip was prepared as shown in Fig. 2c. In the cascade pattern, AS is located 2 mm upstream of DG electrode and connected separately to electric circuits. Pressure-driven flow is generated by a difference in the liquid surface levels of inlet and outlet made of polymethylmethacrylate. A function generator (AFG3022B, Tektronix, USA) connected to the electrodes applied AC electric field into the device with the voltage of 0.4–4.0  $V_{pp}$  and at the frequency of 0.1–100 kHz.

The working fluid was KCl aqueous solution (Wako Pure Chemical Industries, Japan). Electrical conductivity of the solution was set at 4.4 mS/m. As a target particle to be controlled, fluorescent polystyrene particles with the diameter of 0.5, 1.0 or 2.0  $\mu\text{m}$  (FluoSpheres Carboxylate-Modified Microspheres, Invitrogen, USA) were seeded to observe the particle behavior affected by ACEO. Volume fraction of particles in the working fluid was approximately 0.01 %.

## 2.2 Experimental setup

As the measurement method of ACEO velocity, the micron-resolution particle image velocimetry (PIV) was employed in this study (Wereley and Meinhart 2010). This technique is based on the volume illumination and

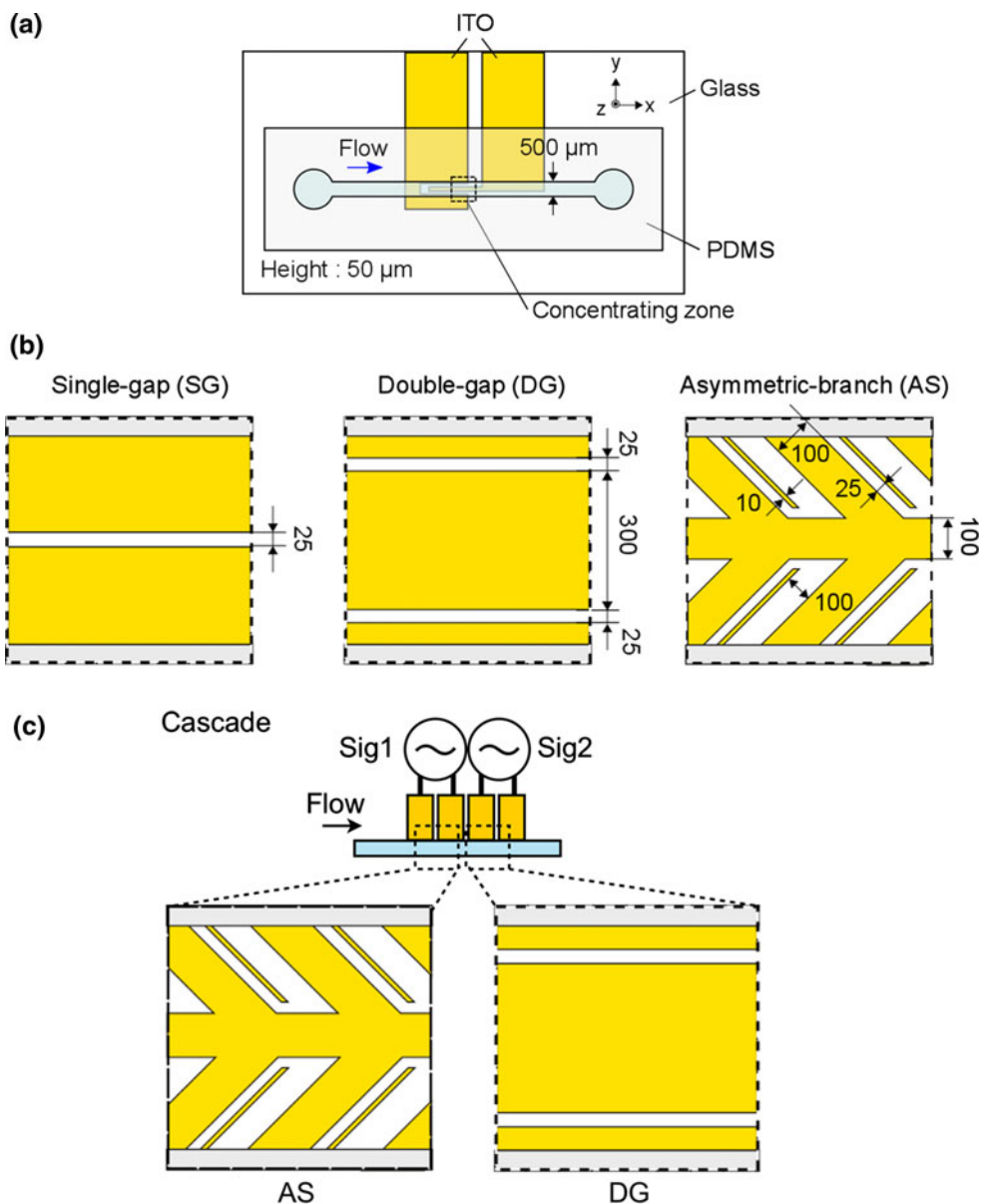
detection of the movement of fluorescent particles in the focal plane of an objective lens. A continuous mercury lamp (Intensilight, Nikon, Japan) is used as an illumination source. The filter cube consisting of an exciter filter, an emitter filter and a dichroic mirror is optimized to perform effective excitation and collection of the fluorescent light for particles. The excitation and emission wavelength of the fluorescent particles are 505 and 515 nm, respectively. The time interval between two images in a pair recorded by a CMOS camera (ORCA-Flash2.8, Hamamatsu Photonics, Japan) was typically 30 ms. The time-average processing between 200 image pairs was performed to reduce the scattering of the measured data due to the random Brownian motion of particles. Since the nonuniformity of particle density in the image used for PIV could affect the correlation-based analytical procedure, the velocity measurements were performed only during the initial stage of concentration, typically less than 10 s after applying voltage, to prevent the nonuniformity.

## 3 Results and discussion

### 3.1 Parametric measurement of ACEO velocity

As mentioned above, there is a discrepancy between theoretical and actual ACEO velocity even with several corrections. Therefore, it is highly needed to experimentally measure the actual ACEO velocity in the fluidic device including its parameter dependence. The substrate in our device has electrode patterns so that the evanescent-wave particle velocimetry (Zettner and Yoda 2003; Huang et al. 2006; Yoda and Kazoe 2011), which can measure a near-wall particle behavior within the range of 100 nm using a thin illumination by an evanescent-wave generated by the total internal reflection of an incident light, is difficult to be applied. In this study, we used the normal micro-PIV system, in which particle movement was measured through the substrate, to measure near-wall particle velocity after the evaluation of effective measurement depth. The focal plane of the objective lens (40 $\times$ , NA 0.60) was set at the

**Fig. 2** **a** Schematic of microfluidic particle concentrator, **b** electrode design; single-gap (SG), double-gap (DG) and asymmetric-branch (AS) and **c** cascade design. The gap spacing in all the devices is 25 μm. In cascade application, AS is located 2 mm upstream of DG connecting separate electric circuits



surface of ITO electrode, and then the time-dependent particle displacement parallel to the wall in quiescent fluid condition was measured using a tracking procedure based on the pattern matching procedure using Gaussian distribution. Figure 3 shows the time revolution of the mean square displacement of 1 μm particles. The similar results obtained at the focal place located 25 μm from the bottom surface is also shown as comparison. The stochastic fluctuation of the particle in bulk condition (focal position  $z = 25 \mu\text{m}$ ) indicates good agreement with the Stokes–Einstein equation in infinite fluid within 1.6 %:

$$\langle \Delta x \rangle^2 = 2D_\infty t = \frac{k_B T}{6\pi r \eta} t \quad (3)$$

where  $D_\infty$  is diffusion coefficient,  $t$  is time,  $k_B$  is Boltzmann’s constant,  $T$  is absolute temperature,  $r$  is

particle radius. The near-wall particle fluctuation shows hindered motion, this is due to the existence of the boundary wall. The correction factor of diffusion coefficient parallel to the wall is presented as follows (Goldman et al. 1967):

$$D^* = \frac{D_\parallel}{D_\infty} = 1 - \frac{9}{16}(r/h) + \frac{1}{8}(r/h)^3 - \frac{45}{256}(r/h)^4 - \frac{1}{16}(r/h)^5 \quad (4)$$

where  $D^*$  and  $D_\parallel$  are corrected diffusion coefficient and diffusion coefficient parallel to the wall, respectively.  $h$  is the distance of particle center from the wall. From the fitting of the experimental data using Eqs. (3) and (4), the effective measurement height of 1.1 μm was obtained. This

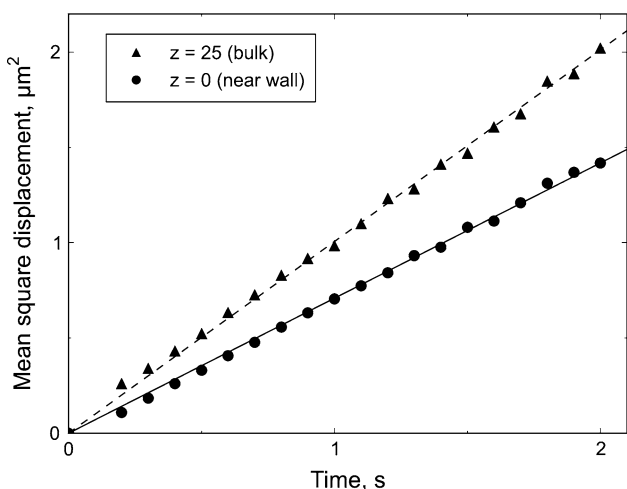


**Fig. 3** Time dependent mean square displacement of particle movement due to Brownian motion. At  $z = 25 \mu\text{m}$ , measured diffusion coefficient matches Stokes–Einstein equation in bulk fluid. Hindered diffusion of near-wall particle ( $z = 0 \mu\text{m}$ ) indicates that actual measurement height in this experiment is  $1.1 \mu\text{m}$  from the bottom wall

value is reasonable considering the effective height of  $1.6 \mu\text{m}$  using the measurement depth (Meinhart et al. 2000; Olsen and Adrian 2000). The effective observation height is estimated as the half the observed depth equal to the half of the measurement depth, namely quarter of the measurement depth.

For figuring out the characteristics of ACEO velocity, especially the parameter dependence on the surface velocity, ACEO velocity on the electrode surface was measured setting the focal plane at the same height as the diffusion measurement. The electrode pattern used here was SG because of its geometrical simplicity. Figure 4a depicts the velocity distribution of the tangential flow induced by ACEO on the electrode surface under voltages from 0.4 to  $2.0 V_{pp}$  at 1.0 kHz. Only one side of SG velocity is shown because of the symmetry. The peak position in ACEO velocity corresponds to the inner edge of electrode ( $y = 12.5 \mu\text{m}$ ). Dependence of the applied voltage on the velocities at three positions of  $y = 12.5, 22.5$  and  $32.5 \mu\text{m}$  is shown in Fig. 4b. The velocity at each position increases with the 2.19, 1.93, and 1.96 power of the voltage, respectively. This tendency agrees well with the linear ACEO theory described in Eq. (1). Figure 5a shows velocities under the frequencies ranging from 0.1 to 10 kHz with a fixed voltage of  $2.0 V_{pp}$ . Under low frequency condition, the tangential fluid flow remains farther from the edge instead of showing some decay in the peak velocity. Figure 5b indicates the relationship between the frequency and the velocities for several positions on the electrode surface. The frequency of the maximum velocity increases with decreasing the distance from the electrode gap.

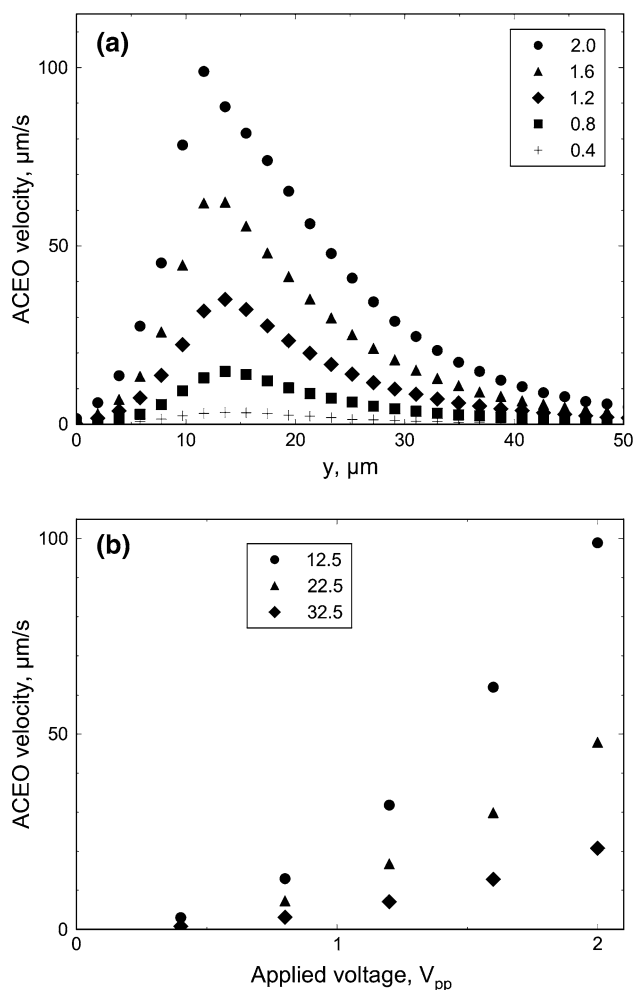


**Fig. 4** ACEO velocity on electrode substrate in SG electrode at a frequency of 1 kHz. **a** Velocity profile at different voltages and **b** voltage dependence at several  $y$  positions

### 3.2 Mechanism of particle collection

ACEO flow advects suspended particles along the electrode surface and accumulates them at a certain location on the electrode surface. The accumulated location is sensitive to the parameters affecting ACEO flow. Figure 6 shows accumulation behaviors of  $1 \mu\text{m}$  fluorescent particles in SG chip at 60 s after applying AC electric field with frequencies from 0.2 to 5.0 kHz at the voltage of  $4.0 V_{pp}$ . The concentrated location indicating the peak intensity shifts close to the center with the increase in the applied frequency as shown in Fig. 6b. Integrals of intensities along  $y$  direction result in almost the same in all the cases. Fluorescence in the inner side of the peak shows lower intensities than the base case that has uniform distribution because of no electric field application, despite of the similar intensities in the outer side of the peak. Therefore, it can be stated that ACEO concentrates particles from inner side toward a specific location. Although this concentration phenomenon



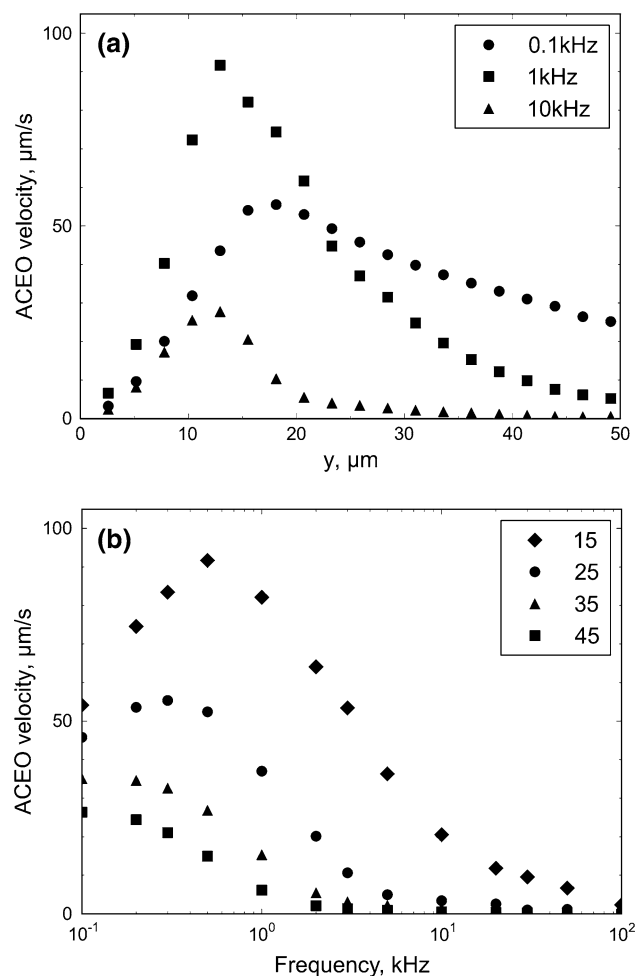


**Fig. 5** Frequency dependence of ACEO velocity in SG electrode. **a** Velocity distribution in spanwise direction and **b** positional dependence ( $y = 15, 25, 35, 45 \mu\text{m}$  from the center of gap)

by ACEO without stagnation area was reported (Ramos et al. 1998), the mechanism has not been fully discussed so far. The insight about the phenomenon is useful for optimized design of ACEO-based particle concentrator. In this study, the mechanism of the particle accumulation is discussed. Since ACEO flow along the electrode surface is tangential, conveyed particles experience no forces normal to the surface except for their spontaneous diffusion. Therefore, we assume that the transportation of particle is effective as far as the convective motion by ACEO overcomes inherent diffusive motion of the particles. A schematic model of the concentrating phenomenon is illustrated in Fig. 7a. As a consequence, particles are concentrated at the balanced position of the advective force and diffusive behavior. Accumulated positions in SG device using different sizes of particles were measured as the peak position of fluorescent intensity. Figure 7b shows the comparison between experimental results and estimation based on the assumption. In this estimation, the accumulation locations were calculated from a balance of diffusive velocity of the

particle using the hindered diffusion coefficient in Eq. (4) and the measured ACEO velocity presented in Sect. 3.1. The diffusive velocity  $V_d$  is given by:

$$V_d = \frac{\sqrt{\langle \Delta x \rangle^2}_{t=t_u}}{t_u} = \sqrt{\frac{2D_{||}}{t_u}} \quad (5)$$

where  $t_u$  is a unit of time.  $D_{||}$  was determined by particle tracking without applied voltage. Particles are collected at farther location from the inner edge of electrode under the lower frequency and larger size. Reasonable agreement between experimental results and estimated locations supports the validity of the assumption. Relatively large difference in  $2 \mu\text{m}$  particle is attributed to the uncertainty of  $z$  position for the measurements. Although having some differences, the balanced accumulation model can explain the mechanism of particle concentration.

### 3.3 Collection performance of parallel double-gap electrode

The collection performance of particle concentration in DG device was evaluated. In DG electrode geometry, two ACEO flows facing each other from both gaps transport particles toward the center of the electrode. When the facing ACEO flow reach the centerline of the electrode, particles are collected on the center of the electrode although there is upward flow normal to the surface. It is reported that particles in the middle of electrode experience a net downward force by positive DEP so that the combination of DEP and ACEO forces causes particles to be concentrated on the electrode surface (Oh et al. 2009). This center collection condition can be obtained under high voltage and low frequency in AC electric field, in which particles can be advected far from the electrode gap. Other cases show separated two concentrated lines with high particle density. Figure 8 indicates comparison of concentrated location from the gap in SG and DG chips under several frequencies. In SG device, the collection location corresponds to the distance from the center gap. The collection locations in both patterns have the same tendency except for low frequency cases in which particles are concentrated at the centerline of electrode (dotted line in the figure). A cross-sectional image of the fluorescent intensity profile shown in Fig. 9a indicates that most of the particles suspended in the solution can be concentrated three-dimensionally on the surface area, less than  $5 \mu\text{m}$  from the wall, where the area corresponds to the stagnation point in ACEO flow field (see Fig. 9b). Here, a different geometry of DG electrode with narrow center electrode of  $50 \mu\text{m}$  wide was used from the reason of observation with high spatial resolution. Concentrated particle image in DG device is shown in Fig. 10. Most of the suspended particle

**Fig. 6** Behaviors of particle concentration in SG chip at different frequencies with a voltage of  $4V_{pp}$ . **a** Fluorescent image from particles and **b** fluorescent intensity profile at half of the channel. Base means the case without applying voltage

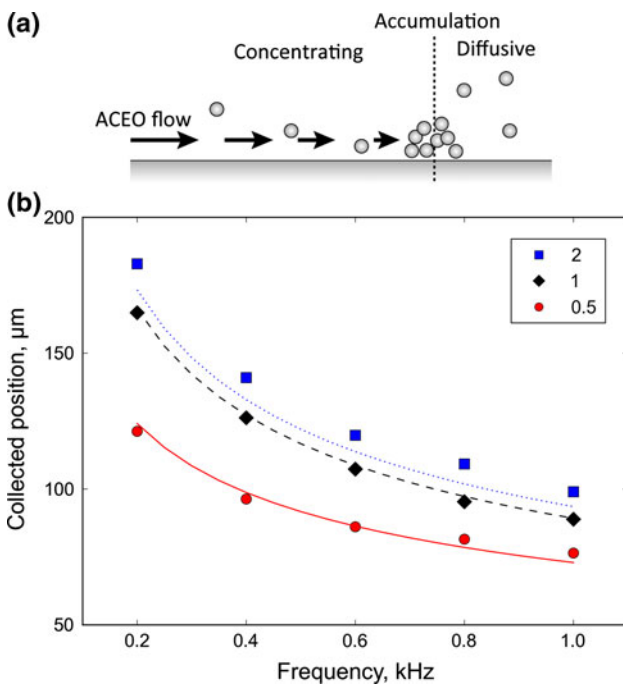
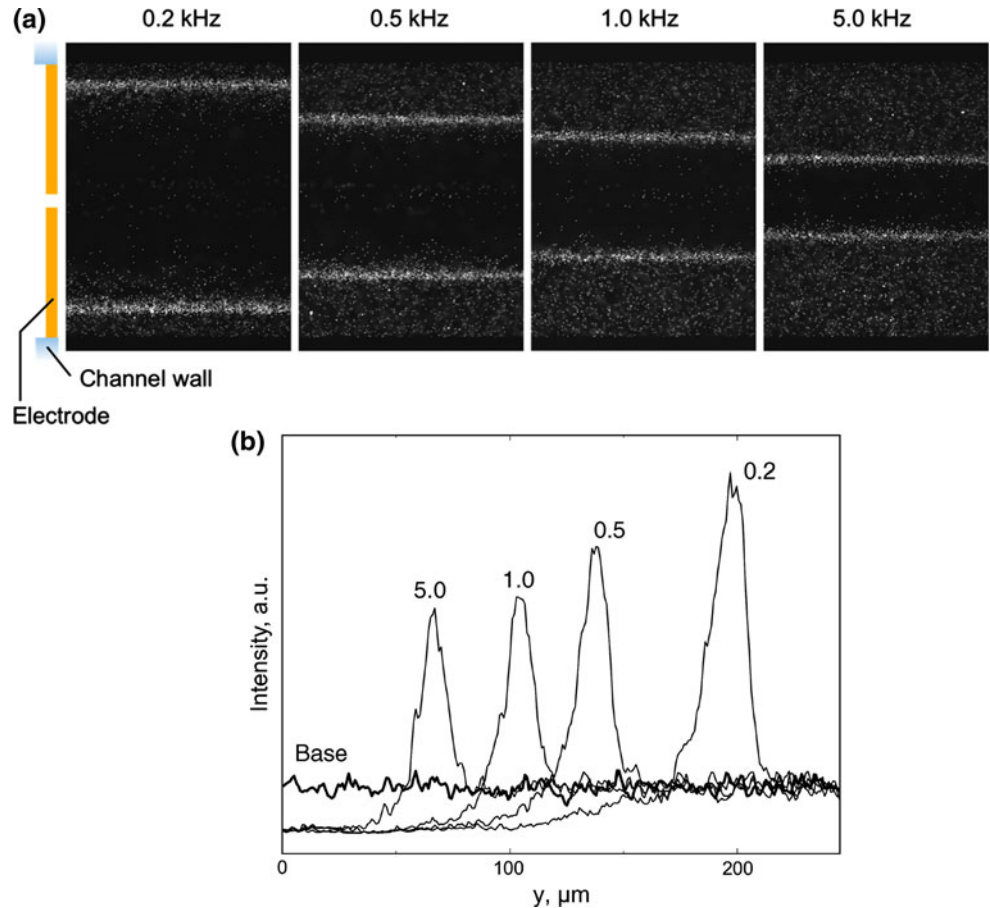


**Fig. 7** Particle collection by ACEO in SG device. **a** Schematic model of accumulation based on the ‘balanced assumption’ and **b** experimental results of collected position under different frequencies and particle sizes. Lines shown in the figure corresponds calculated positions

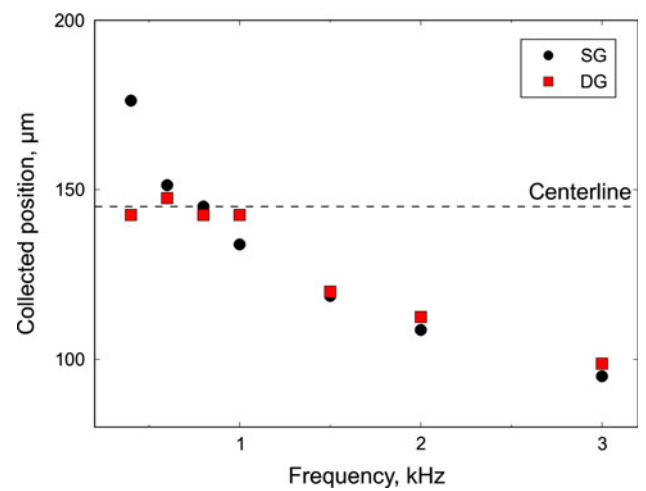


**Fig. 8** Collected positions in SG and DG devices under different frequencies

in the channel was concentrated around center of the electrode. However, at each sidewall region there is a dense area of particles which is attributed to counter ACEO flow. This DG chip can concentrate particles above the center electrode (concentration zone in upper figure), and outside particles are moved close to sidewall (scattering zone).

Since the concentration capability of DG geometry is valid for particles passing above the center electrode, the collection factor for all particles in the 500  $\mu\text{m}$  channel is limited as much as 60 %.

### 3.4 Cascade ACEO application for improved concentration

To avoid particle flowing in scattering zone, an additional scheme to control initial position of particles is required. In order to improve the limit of concentration rate in DG chip due to its geometry, we investigated two approaches; one is the use of sheath flow to focus the particle flow and the other is the cascade ACEO application using AS and DG electrode patterns. The collection performance of particle concentration in DG device was evaluated by particle counting. Particle distribution in spanwise direction for sheathed particle flow and ACEO concentration with sheathed flow are indicated in Fig. 11. Applied frequency and voltage were 200 kHz and 4.0  $V_{pp}$ . Sheathed particle flow was achieved to feed sheath liquid from both sides of the channel using a branched channel, and the width of sheathed particle flow was controlled by the flow-rate ratio of particle and sheath flow widely used in microfluidic flow cytometry (Chung and Kim 2007; Ateya et al. 2008). The width of the channel after junction was 500  $\mu\text{m}$ . The sheath flow focuses particle flow within the center electrode region (dotted line in the figure), and ACEO effectively collects particles. As a result, overall concentration efficiency, defined the count rate within 50  $\mu\text{m}$  area at the center, was 81.2 %. This value overcomes the intrinsic limit of DG chip of 60 %.

AS electrode was designed to induce ACEO flow to collect gently particles around the sidewall region toward above the center region to promote concentration functionality of DG. Figure 12 shows concentration performances of DG, AS, and cascade use of AS and DG. Here, different electric fields were separately applied in AS and DG electrode; 2.5  $V_{pp}$  and 0.7 kHz for AS electrode, and 4.0  $V_{pp}$  and 0.1 kHz for DG. It is clarified that the most of the particles passing entire spanwise area in the channel are collected at the center area very sharply without the sidewall concentration in the case of the cascade case. The peak count rate of the cascade device was enhanced to 21.6 % while DG and AS showed the peak values of 17.6 and 3.6 %, respectively. The full width at half maximum (FWHM) of concentrated particle distribution in the cascade chip was approximately 3  $\mu\text{m}$ , equal to 0.6 % of the channel width. The count rates obtained in this experiment are summarized in Table 1. Center and sidewall area means 50  $\mu\text{m}$  at the center and 50  $\mu\text{m}$  from the sidewall, respectively. The cascade design for ACEO concentrator distinctively prevents particle flowing the scattering zone

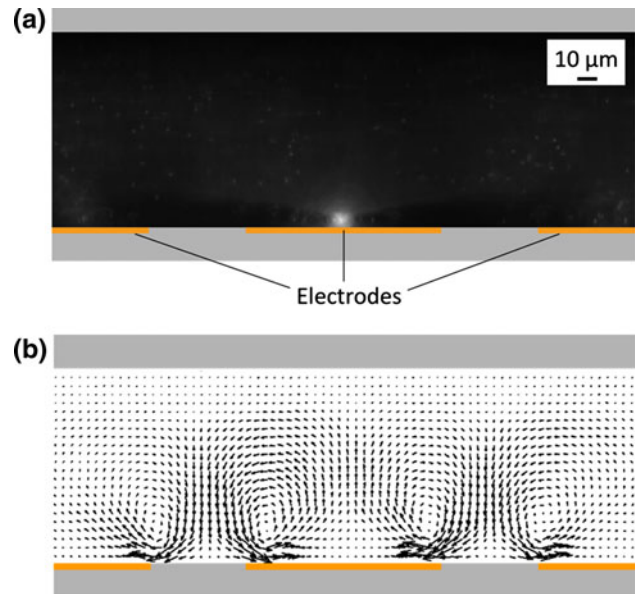


**Fig. 9** Cross-sectional view of particle concentration by ACEO in DG device. **a** Fluorescent particle distribution and **b** velocity field measured by micro-PIV. Concentration is performed only on the surface area within the height less than 5  $\mu\text{m}$ . Here, different DG electrode with 50  $\mu\text{m}$  wide center electrode is used to observe whole phenomena in an image with high resolution

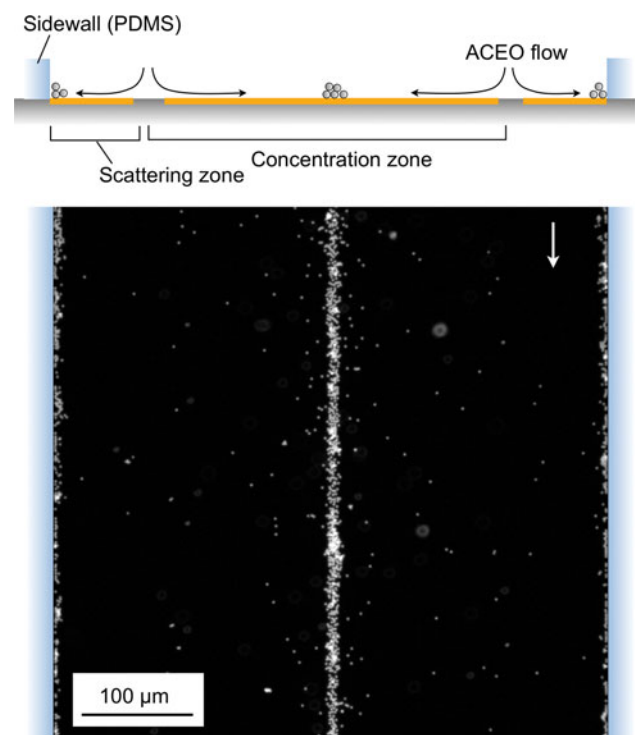


**Fig. 10** Concentration performance of ACEO in DG device. Most of flowing particle in the channel is concentrated around center of the electrode. At each sidewall region, there is a dense particle area which is attributed to counter ACEO flow. This DG chip can concentrate particles above the center electrode (concentration zone in upper figure)



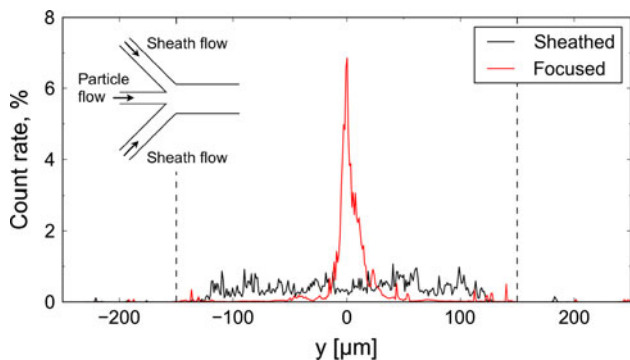


**Fig. 11** Particle distribution in spanwise direction for sheathed particle flow and ACEO concentration with sheathed flow. Sheathed flow focuses particle flow within the center electrode region (dotted line), and ACEO in DG electrode effectively collects particles. Overall concentration efficiency is 81.2 %, which overcomes the intrinsic limit of DG chip

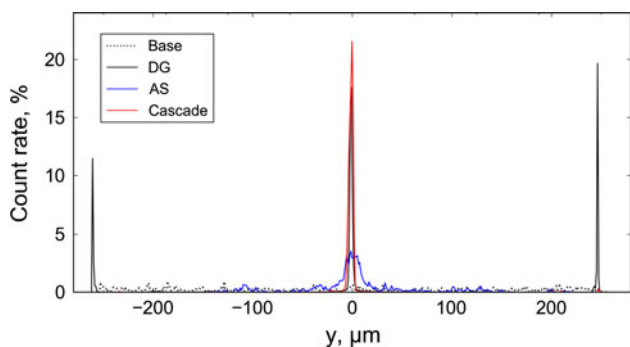


**Fig. 12** Performance of particle concentration in DG, AS and cascade device. AS is located upstream of DG in cascade. Base means data without applying electric filed. Application of cascade electrode geometry enhances concentrating ability of DG avoiding scattering zone near sidewall. The result indicates uniform particle dispersion FWHM (full width at half maximum) of concentrated profile is approximately 3 μm

**Table 1** Particle concentration rate at center and sidewall area

	Count rate (%)			
	Base	DG	AS	Cascade
Center area	11.6	56.3	65.0	98.4
Sidewall area	3.6	48.2	1.2	0.9

and collects 98.4 % of the particles in the channel into the center area. In addition, considering the vertical concentration shown in Fig. 9, three-dimensional concentrating factor can be estimated as more than 700. This AC electrokinetic method for 3D particle focusing method can be potentially used in impedance cytometry (Gawad et al. 2001; Cheung et al. 2010) or electrochemical detection (Goral et al. 2006; Zimmerman 2011).

### 4 Conclusions

In this study, characteristics of the ACEO flow for particle concentration in a microchannel have been investigated. The transportation of particles by ACEO advection causes an accumulation of particle on the surface of electrode depending on applied voltage, frequency, and properties of the medium, but not on the particle properties. The position where particles are collected can be explained as the balance of attenuation in ACEO flow and the near-wall hindered diffusion of particles close to the wall. Experimental and estimated positions of particle collection matched well. The accumulation location in double-gap electrode chip varies its condition based on the electrode geometry and predictable collected distance in single-gap electrode case. This would be helpful to design and optimize the microfluidic chip with particle manipulation based on ACEO flow. The concentration performance of the double-gap electrode has a limitation of effective spatial range, and this can be overcome to apply sheath flow or utilize cascade electrode upstream of DG electrode. Overall concentration rate in the cascade chip was 98.4 %, much larger than DG chip. This cascade ACEO concentrator provides efficient sheathless concentration for particles in the microfluidic platform with low voltage application. These results imply the validity of the innovative particle concentration by ACEO for highly sensitive and accurate detection of rare samples.

**Acknowledgments** This work was supported by Specified Research Grant in Tokyo University of Science. A part of microfabrication was performed in Center for Nano Lithography and Analysis, The University of Tokyo, supported by the Ministry of Education, Culture, Sports, Science and Technology (MEXT), Japan.

### References

Ajdari A (2000) Pumping liquids using asymmetric electrode arrays. *Phys Rev E* 61:R45–R48

Ateya DA, Erickson JS, Howell PB Jr, Hilliard LR, Golden JP, Ligler FS (2008) The good, the bad, and the tiny: a review of microflow cytometry. *Anal Bioanal Chem* 391:1485–1498

Bazant MZ, Thornton K, Ajdari A (2004) Diffuse-charge dynamics in electrochemical systems. *Phys Rev E* 70:021506

Bhatt KH, Grego S, Velev OD (2005) An AC electrokinetic technique for collection and concentration of particles and cells on patterned electrodes. *Langmuir* 21:6603–6612

Castellanos A, Ramos A, González A, Green NG, Morgan H (2003) Electrohydrodynamics and dielectrophoresis in microsystem: scaling laws. *J Phys D* 36:2584–2597

Chen L, Prest JE, Fielden PR, Goddard NJ, Manz A, Day PJR (2006) Miniaturized isotachopheresis analysis. *Lab Chip* 6:474–487

Cheung KC, Berardino MD, Kampmann GS, Hebeisen M, Pierzchalski A, Bocsi J, Mittag A, Tárnok A (2010) Microfluidic impedance-based flow cytometry. *Cytom Part A* 77A:648–666

Chung TD, Kim HC (2007) Recent advances in miniaturized microfluidic flow cytometry for clinical use. *Electrophoresis* 28:4511–4520

- Cui H, Dutta P, Ivory CF (2007) Isotachophoresis of proteins in a networked microfluidic chip: experiment and 2-D simulation. *Electrophoresis* 28:1138–1145
- Fiedler S, Shirley SG, Schnelle T, Fuhr G (1998) Dielectrophoretic sorting of particles and cells in a microsystem. *Anal Chem* 70:1909–1915
- Gawad S, Schild L, Renaud P (2001) Micromachined impedance spectroscopy flow cytometer for cell analysis and particle sizing. *Lab Chip* 1:76–82
- Godin J, Chen C, Cho SH, Qiao W, Tsai F, Lo Y (2008) Microfluidics and photonics for bio-system-on-a-chip: a review of advancements in technology towards a microfluidic flow cytometry chip. *J Biophoton* 1:355–376
- Goldman AJ, Cox RG, Brenner H (1967) Slow viscous motion of a sphere parallel to a plane wall—I motion through a quiescent fluid. *Chem Eng Sci* 22:637–651
- Goral VN, Zaytseva NV, Baeumner AJ (2006) Electrochemical microfluidic biosensor for the detection of nucleic acid sequences. *Lab Chip* 6:414–421
- Gregersen MM, Olesen LH, Brask A, Hansen MF, Bruus H (2007) Flow reversal at low voltage and low frequency in a microfabricated AC electrokinetic pump. *Phys Rev E* 76:056305
- Hu M, Yan J, He Y, Lu HH, Weng L, Song S, Fan C, Wang L (2010) Ultrasensitive, multiplexed detection of cancer biomarkers directly in serum by using a quantum dot-based microfluidic protein chip. *NANO* 4:488–494
- Huang P, Guasto JS, Breuer KS (2006) Direct measurement of slip velocities using three-dimensional total internal reflection velocimetry. *J Fluid Mech* 566:447–464
- Jacobson SC, Ramsey JM (1995) Microchip electrophoresis with sample stacking. *Electrophoresis* 16:481–486
- Jones TB (ed) (1995) *Electromechanics of particles*. Cambridge University Press, New York
- Lian M, Islam N, Wu J (2006) Particle line assembly/patterning by microfluidic AC electroosmosis. *J Phys Conf Ser* 34:589–594
- Lin CC, Hsu JL, Lee GB (2011) Sample preconcentration in microfluidic devices. *Microfluid Nanofluid* 10:481–511
- Meinhart CD, Wereley ST, Gray MHB (2000) Volume illumination for two-dimensional particle image velocimetry. *Meas Sci Technol* 11:809–814
- Melvin EM, Moore BR, Gilchrist KH, Grego S, Velev OD (2011) On-chip collection of particles and cells by AC electroosmotic pumping and dielectrophoresis using asymmetric microelectrodes. *Biomicrofluidics* 5:034113
- Nagrath S, Sequist LV, Maheswaran S, Bell DW, Irimia D, Ulkus L, Smith MR, Kwak EL, Digumarthy S, Muzikansky A, Ryan P, Balis UJ, Tompkins RG, Haber DA, Toner M (2007) Isolation of rare circulating tumour cells in cancer patients by microchip technology. *Nature* 450:1235–1239
- Neethirajan S, Kobayashi I, Nakajima M, Wu D, Nandagopaldand S, Lin F (2011) Microfluidics for food, agriculture and biosystems industries. *Lab Chip* 11:1574–1586
- Oh J, Hart R, Capurro J, Noh HM (2009) Comprehensive analysis of particle motion under non-uniform AC electric fields in a microchannel. *Lab Chip* 9:62–78
- Olesen LH, Bruus H, Ajdari A (2006) AC electrokinetic micropumps: the effect of geometrical confinement, Faradaic current injection, and nonlinear surface capacitance. *Phys Rev E* 73:056313
- Olesen LH, Bazant MZ, Bruus H (2010) A strongly nonlinear dynamics of electrolytes in large ac voltages. *Phys Rev E* 82:011501
- Olsen MG, Adrian RJ (2000) Out-of-focus effects on particle image visibility and correlation in microscopic particle image velocimetry. *Exp Fluids* 29:S166–S174
- Pamme N (2006) Magnetism and microfluidics. *Lab Chip* 6:24–38
- Prat ED, Huang C, Hawkins BG, Gleghorn JP, Kirby BJ (2011) Rare cell capture in microfluidic devices. *Chem Eng Sci* 66:1508–1522
- Ramos A, Morgan H, Green NG, Castellanos A (1998) AC electrokinetics: a review of forces in microelectrode structures. *J Phys D* 31:2338–2353
- Sequist LV, Nagrath S, Toner M, Haber DA, Lynch TJ (2009) The CTC-chip: an exciting new tool to detect circulating tumor cells in lung cancer patients. *J Thorac Oncol* 4:281–283
- Shiddiky MJA, Shim YB (2007) Trace analysis of DNA: preconcentration, separation, and electrochemical detection in microchip electrophoresis using Au nanoparticles. *Anal Chem* 79:3724–3733
- Sueyoshi K, Kitagawa F, Otsuka K (2008) Recent progress of online sample preconcentration techniques in microchip electrophoresis. *J Sep Sci* 31:2650–2666
- Sun T, Morgan H (2010) Single-cell microfluidic impedance cytometry: a review. *Microfluid Nanofluid* 8:423–443
- Warrick J, Casavant B, Frisk M, Beebe D (2010) A microfluidic cell concentrator. *Anal Chem* 82:8320–8326
- Watarai H, Suwa M, Iiguni Y (2004) Magnetophoresis and electro-magnetophoresis of microparticles in liquids. *Anal Bioanal Chem* 378:1693–1699
- Wereley ST, Meinhart CD (2010) Recent advances in micro-particle image velocimetry. *Annu Rev Fluid Mech* 42:557–576
- Whitesides GM (2006) The origins and the future of microfluidics. *Nature* 442:368–373
- Yeo LY, Chang HC, Chan PPY, Friend JR (2011) Microfluidic devices for bioapplications. *Small* 7:12–48
- Yoda M, Kazoe Y (2011) Dynamics of suspended colloidal particles near a wall: implications for interfacial particle velocimetry. *Phys Fluid* 23:111301
- Zettner CM, Yoda M (2003) Particle velocity field measurements in a near-wall flow using evanescent wave illumination. *Exp Fluid* 34:115–121
- Zhang C, Khoshmanesh K, Mitchell A, Kalantar-zadeh K (2010) Dielectrophoresis for manipulation of micro/nano particles in microfluidic systems. *Anal Bioanal Chem* 396:401–420
- Zimmerman WB (2011) Electrochemical microfluidics. *Chem Eng Sci* 66:1412–1415